From seasonal flood pulse to seiche: Multi-frequency waterlevel fluctuations in a large shallow tropical lagoon (Nokoué Lagoon, Benin)

Alexis Chaigneau, Victor Okpeitcha, Yves Morel, Thomas Stieglitz, Arnaud Assogba, Morgane Benoist, Pierre Allamel, Jules Honfo, Thierry Derol Awoulmbang Sakpak, Fabien Rétif, et al.

From seasonal flood pulse to seiche: Multi-frequency water-level fluctuations in a large shallow tropical lagoon (Nokoué Lagoon, Benin).

Alexis CHAIGNEAU[a,b,c,*], Victor OKPEITCHA[d,c,b], Yves MOREL[a], Thomas STIEGLITZ[e], Arnaud ASSOGBA[b], Morgane BENOIST[a,b], Pierre ALLAMEL[f], Jules HONFO[c], Thierry Derol AWOULMBANG SAKPAK[g], Fabien RÉTIF[h], Thomas DUHAUT[a], Christophe PEUGEOT[i], Zacharie SOHOU[b]

[a] Laboratoire d'Études en Géophysique et Océanographie Spatiale (LEGOS), Université de Toulouse, CNES, CNRS, IRD, UPS, Toulouse, France

[b] Institut de Recherches Halieutiques et Océanologiques du Bénin (IRHOB), Cotonou, Bénin,

[c] International Chair in Mathematical Physics and Applications (ICMPA–UNESCO Chair), University of Abomey-Calavi, Cotonou, Benin

[d] Laboratoire d'Hydrologie Appliquée (LHA), Institut National de l'Eau (INE), African Centre of Excellence for Water and Sanitation (C2EA), Université d'Abomey Calavi, Bénin

[e] Aix-Marseille Université, CNRS, IRD, INRAE, Coll France, CEREGE, Aix-en-Provence, France

[f] STATMarine, La Seyne Sur Mer, France

[g] Laboratoire des Technologies et Sciences Appliquées, Université de Douala, Douala, Cameroun

[h] RETIF FABIEN PHILIAN, Montferrier sur Lez, France

[i] Hydrosciences Montpellier (HSM), Université de Montpellier, CNRS, IRD, Montpellier, France

[*]Corresponding Author: alexis.chaigneau@ird.fr

Abstract

This study investigated the main water-level (WL) variability modes of Nokoué Lagoon in Benin (West-Africa). The average WL ranges between 1.3 and 2.3 m between the low- and high-water seasons. Seasonal as well as weak interannual variations between 2018 and 2019 are driven by rainfall regime over the catchment and associated river inflow. At sub-monthly scales, the lagoon is tidally choked: ocean tides can reach 90 cm, whereas in the lagoon semi-diurnal and diurnal tides hardly reach few centimeters. Choking conditions vary with river inflow and ocean tide amplitude, correctly represented by a simple tidal choking model. Diurnal modulation and asymmetry of the tide are stronger (weaker) during high (low) water period. We also observed WL variations of ±5-10 cm at a fortnightly frequency, stronger during wet (high-water) season. Superimposed on the seasonal, fortnightly and tidal WL variations, we further observed short-term high-frequency seiche events. Mostly observed during dry (low-water) conditions, they are characterized by typical standing-wave oscillations of 5-10 cm amplitudes and 3 h periods. They are forced by the passage of fast-moving squall-lines that induce strong wind variations, heavy rainfalls and rapid drop-off of the air temperature. Results obtained in this study provide useful metrics for the validation of flood forecasting models to be implemented in Benin, and elsewhere on the West African coastline.

Keywords: Water-levels; Lagoons; Tides; Seiches; Nokoué; Wavelet analysis.

1. Introduction

In the eastern tropical Atlantic Ocean, the coastal zone bordering the Gulf of Guinea include a series of coastal lagoons of varying sizes (Allersma and Tilmans, 1993; Lalèyè et al., 2007; Adite and Winemiller, 1997; Adite et al., 2013). These lagoons are often the main mixing zone of continental freshwater and coastal seawater, supporting some of the most productive aquatic ecosystems in the world (Knoppers, 1994; Valiela, 1995; Duck and da Silva, 2012). These coastal systems support important ecosystem services for the local populations who benefit from these natural or semi-natural areas through different activities (fishing, tourism, sand and/or salt extraction, etc.) (Djihouessi et al., 2017; Newton et al., 2018).

Among the various Beninese coastal lagoons, Nokoué Lagoon (Figure 1) is the largest and most exploited of the country's water bodies (Lalèyè et al., 1995; 2003). This lagoon, which is also one of the most productive in West Africa (Lalèyè et al., 2007), is at the heart of important ecological and socio-economic issues. It is part of the RAMSAR site #1018, recognized to be of international importance for its various ecosystems that include flood plains, mangroves, floating vegetation, and diverse fauna. This lagoon also hosts several lacustrine villages inhabited by more than 60000 people living in stilt dwellings (Principaud, 1995). These local populations depend on this water body not only for fishing, which provides ~15000 tons of fish per year (Principaud, 1995), but also for domestic water supply, agriculture, market gardening, animal husbandry, etc. But the Nokoué Lagoon, also bordered by 3 major urban centers (Cotonou, Abomey-Calavi, and Sémè Podji) totalizing more than 1.5 million inhabitants, is strongly impacted by various anthropogenic pollution sources. For instance, the lagoon is the receptacle of numerous urban drains and direct discharge by the surrounding populations of various wastes which has led to a deterioration of the water quality (Adjahouinou et al., 2012; 2014; Aina et al., 2012a; 2012b). In addition, Nokoué Lagoon is also embedded within the 500 km long West African coastal water corridor that stretches from Lagos (Nigeria) to Accra (Ghana). This coastal corridor is projected to become the largest African urbanized area (Choplin, 2019), a development that will threaten the lagoons' ecosystems and their service function. The planning and implementation of coastal management strategies requires a comprehensive knowledge of processes involved in the physical, chemical and ecological dynamics of the Nokoué Lagoon.

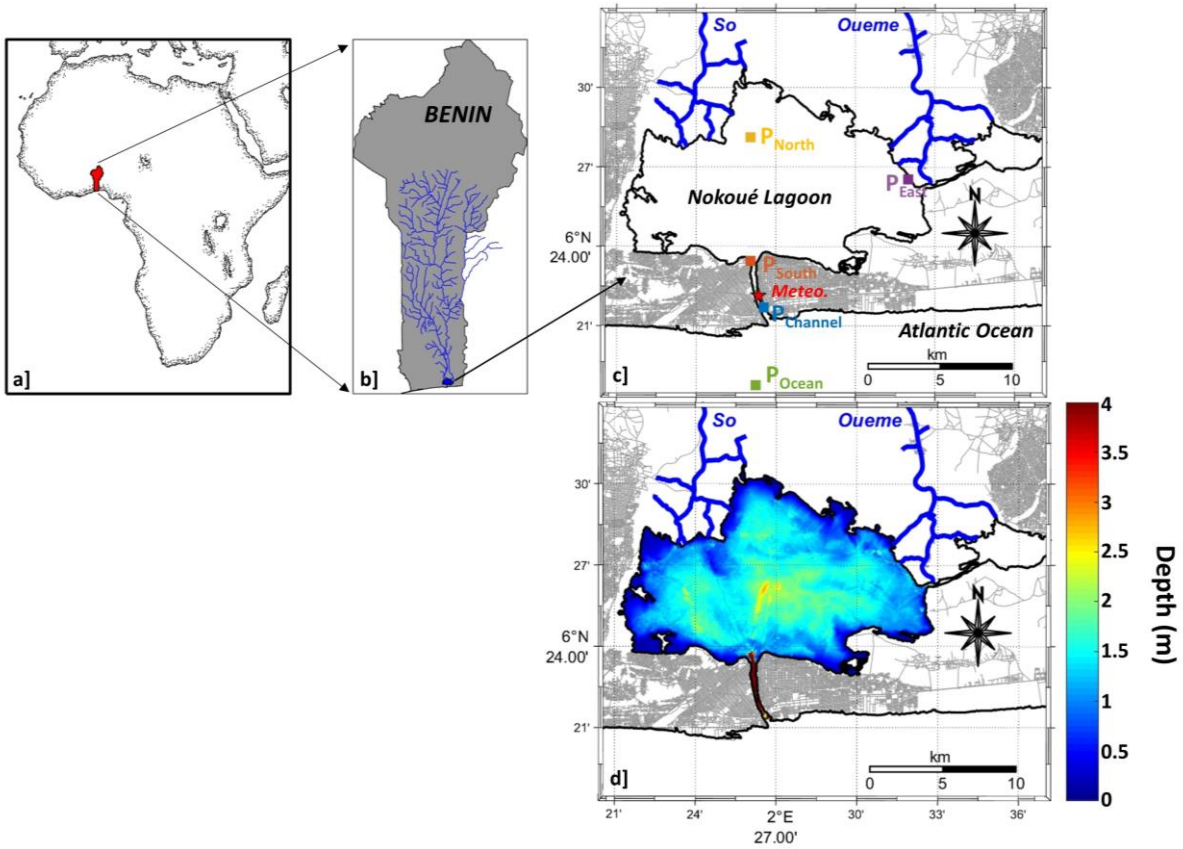

Figure 1. Geographical location of the Nokoué Lagoon in Bénin. a] Benin in West-Africa. b] Hydrological network of the Sô and Ouémé river catchment basins. c] Nokoué Lagoon and position of the water-level stations (colored squares); the location of the weather station is indicated by a red star. d] Bathymetry corresponding to the mean water-level observed in low water season and obtained from a spatial interpolation of ~123000 depth soundings.

One of the key parameters of coastal lagoon dynamics is the water level (WL) whose variations are mainly subject to the triple influence of (i) ocean tides, (ii) the hydrological variability of the catchment and (iii) direct rainfall contributions. Generally, high WL is associated with strong freshwater river discharge and low WL with time periods when salty oceanic water penetrates into the lagoon. First, WL fluctuations impact the lagoon circulation and consequently the turnover, residence or flushing times and therefore the dispersion or retention of pollutants. Second, the lagoon WL determines the exchange of properties between the continent and the ocean and controls the ecosystems by various direct or indirect processes. In a direct way, WL fluctuations control the salinity of the lagoon (e.g. Djihouessi and Aina, 2018), which directly impacts the ecosystem composition from plankton to fish (Le Barbé et al., 1993; Gnohossou, 2006; Adandedjan et al., 2017; Odountan et al., 2019; Laléyè et al., 2003; 2005). In an indirect way, WL variations impact lagoon and sediment dynamics by modifying erosion and sedimentation zones and the rate of sediment resuspension. Thus, turbidity and the availability of light on the vertical can vary according to the WL,

which can modify the structure of biological communities, particularly phytoplankton (Evtimova and Donohue, 2016). Similarly, WL fluctuations are correlated with modifications of nutrient concentrations, mixing and vertical stratification in the water column, eventually affecting the development, distribution and dilution of organisms as observed in other water bodies (e.g. Lobo et al., 2018; Stević et al., 2013).

Third, in addition to having direct or indirect effects on the ecosystem, variations in the WL of Nokoué Lagoon can have dramatic repercussions on local populations. Indeed, lacustrine villages and urbanized areas adjacent to the lagoon episodically experience flooding linked to major watershed floods and the regular overflow of the lagoon. For instance, in 2010, flooding killed tens of people and affected 360 000, leaving 100 000 homeless (World Bank, 2011; Ahouangan et al., 2014; Biao, 2017). More recently, in October-November 2019, the floods, less intense but spread over several weeks, also caused extensive damage and affected tens of thousands of households.

Finally, variations in the WL may also impact the quality of the groundwater that is exploited by residents bordering the lagoon, who use this unregulated shallow groundwater resource for domestic purposes, including drinking water supplies (Houéménou et al., 2020).

Only few studies described some patterns of WL fluctuations in Nokoué Lagoon (e.g. Le Barbé et al., 1983; Zandagba et al., 2016; Djihouessi and Aina, 2018). Based on observations obtained over isolated and short time periods, the WL variability is poorly described: a seasonal increase of ~50-70 cm is mentioned during the flood season (Le Barbé et al., 1983; Djihouessi and Aina, 2018) and tidal amplitudes of 10-25 cm were observed in the Cotonou channel (Zandagba et al., 2016). This study aims to fill this gap and to investigate WL variations in this lagoon at different time scales from a 2-year in-situ dataset at 20 min sampling, and to determine the main physical mechanisms governing the observed fluctuations.

2. Material and methods

2.1. Study area and hydrology

Nokoué is a costal lagoon that extends about 20 km from east to west along the coast and 11 km from south to north (Figure 1), covering an average area of ~170 km^2 (Texier et al., 1980; Le Barbé et al., 1993; Mama et al., 2011; Djihouessi et al., 2019). Two main rivers flow into the lagoon on its northern shore, the Sô river, draining a relatively

small catchment area of ~1000 km^2, and the Ouémé river, the largest Beninese river, which drains a catchment area of ~50000 km^2 (Le Barbé et al., 1993; Djihouessi et al., 2017). The Sô and the lower Ouémé valley flow into the Nokoué Lagoon forming a large flooded deltaic plain (e.g. Le Barbé et al., 1993). A third river, the Djonou, whose extension and flow are much smaller, also contributes to the freshwater inflow in the lagoon's southwestern part (Djihouessi and Aina, 2018).

On its southern part, Nokoué Lagoon is connected with the Atlantic Ocean by the ~280 m wide and ~4 km long Cotonou channel (Texier et al., 1980; Le Barbé et al., 1993). Through this relatively narrow channel, exchanges of fresh and salt water take place at the rhythm of the tides and the hydrological regime. Since the channel's construction in 1885, the previously unconnected 'Lake' Nokoué (as it is still known in colloquial language) is today an extensive lagoon that exhibits important salinity variations (e.g. Okpeitcha et al., in review).

On the eastern side, Nokoué Lagoon is connected to the Porto-Novo lagoon (35 km^2) via the ~4 km long Totchè channel. Porto-Novo lagoon extends eastward into a narrow coastal channel that discharges in the Atlantic Ocean at Lagos (Nigeria) at a distance of ~100 km from Nokoué Lagoon, with little effect on the dynamics and WL of Nokoué Lagoon (Texier et al., 1980; Le Barbé et al., 1993).

On seasonal scales, the lagoon's hydrological regime is driven by the West African summer monsoon related to the meridional shift of the intertropical convergence zone (ITCZ) and the associated intense tropical rain belt (Sultan and Janicot, 2000; Gu and Adler, 2004), resulting in two rainy and two dry seasons. The main rainy season extends from April-May to late July when the ITCZ moves northward from its near-equatorial southernmost position, while the second shorter and less intense rainy period extends from late September to November when the ITCZ migrates southward from its northernmost position (e.g. N'Tcha M'Po et al., 2017; Ahokpossi, 2018). However, this double rainy season and associated local rainfalls only slightly influence the WL of the Nokoué Lagoon that is more subject to the hydrology of the central part of Benin, where the main area of the Ouémé catchment takes place (e.g. Colleuil, 1987; see also Figure 1b). This latter region is characterized by a single rainy season, with maximum precipitation between July and October (Biao, 2017; Ahokpossi, 2018; Lawin et al., 2019, Colleuil, 1987). The maximum discharge into the lagoon between September and November is unknown (rivers ungauged in the coastal region) and varies, depending on

authors, from ~400 m^3 s^{-1} (Le Barbé et al., 1993; Djihouessi and Aina, 2018) to more than 1000 m^3 s^{-1} (Lawin et al., 2019). This river discharge produces a complete desalinization of the Nokoué Lagoon and a strong increase of its volume (Texier et al., 1980; Colleuil, 1987; Djihouessi and Aina, 2018).

Figure 1d shows the bathymetry of the Nokoué Lagoon corresponding to the mean WL observed during low-water season in March-April. It was constructed using ~123000 depth soundings recorded with a Garmin GPSmap 421S echosounder and corrected for tidal and seasonal fluctuations. The mean and maximum depth is 1.3 m and 2.9 m, respectively. The lagoon deepens towards the Cotonou channel where the mean and maximum depths increase to ~3 m and ~8 m, respectively (Figure 1d).

2.2. Water level and atmospheric data

WL data was acquired by 4 pressure sensors deployed in the Cotonou channel and Nokoué Lagoon for a 2-year period (Figure 1c). Three of them ($P_{Channel}$, P_{South}, P_{North}) were located along a South-North axis whereas the 4th sensor (P_{East}) was deployed East of the lagoon. More precisely, $P_{Channel}$ is located at 1.5 km from the coastal ocean; P_{South} is located at the lagoon entrance; P_{North} is located 8.5 km North of P_{South} and at ~2 km from the Sô river; finally, P_{East} is located 11.3 km southeast of P_{North} and 12.3 km northeast of P_{South}.

Each of the 4 stations consisted of an Onset HOBO U20L-01 WL logger anchored at 20-30 cm from the bottom in a perforated PVC tube of 7-cm outside diameter. Data were recorded continuously at 20-min interval between February 2018 and January 2020, with a typical accuracy of ±1 cm and a maximum error of 2 cm (https://www.onsetcomp.com/files/manual_pdfs/17153-G%20U20L%20Manual.pdf) (Wilson et al., 2016; Guragai et al., 2018).

From 30 August 2018, a Davis Vantage Pro2 weather station was installed on the roof of the Benin Institute of Fisheries and Oceanographic Research (IRHOB; Figure 1c) also recording at 20-min interval. Some of the atmospheric parameters (air temperature and humidity, precipitation rates, and winds) are used to explore the forcing mechanisms involved in high frequency WL variations (Section 3.4). However, atmospheric pressure data were overall used to correct the WL between September 2018 and January 2020. Before September 2018, WL was not corrected for barometric fluctuations, but this does not significantly alter the results and main conclusions drawn

in this study. Indeed, atmospheric pressure, that varied between 1004 mbar and 1019 mbar over the available time period, exhibits two main modes of variability. First, at seasonal scale, atmospheric pressure varies by ~4 mbar, being minimum in April and maximum in August. This corresponds to a WL correction of ~4 cm which is weak compared with the seasonal WL variations of ~90 cm observed in this study (Section 3.1). Second, the stronger atmospheric pressure variability is observed at diurnal and semi-diurnal periodicities, with mean and maximum variations of ~3 and 6 mbar, respectively. This corresponds to WL variations of ~3-6 cm, of the same order than the tidal amplitudes observed in the lagoon. Thus, the tide characteristics in the lagoon (Section 3.3), are investigated using WL data corrected from inverse barometer effects (September 2018-December 2019).

Raw pressure data are converted to relative WLs corresponding to the height above the instrument. For each station, as no absolute vertical datum exists, the relative WLs are expressed in terms of anomalies, computed by subtracting the 20-min measurements from the seasonal mean calculated over low-water period of 2018.

No continuous in-situ ocean tide data is available. We therefore used the tidal heights computed from the last Finite Elements Solution for ocean tide (FES2014) on a 1/16° × 1/16° grid (http://www.aviso.altimetry.fr/en/data/products/auxiliary-products/global-tide-fes.html) (Carrere et al. 2016; Lyard et al. 2020). Thus, WL anomaly timeseries at P_{Ocean} (Figure 1c) was reconstructed using the 34 tidal constituents (amplitudes and phases) computed from FES2014. P_{Ocean} is located ~5.5 km to the southeast of $P_{Channel}$ (Figure 1c). FES WL at P_{Ocean} compared well with independent but irregular in-situ WL data acquired at the autonomous port of Cotonou in 2018-2019 by its hydrographic service. The correlation coefficient, mean difference, normalized root-mean-square error, and ratio of standard deviations between both datasets are 0.99, 0.02 cm, 2.7%, and 0.99, respectively.

2.3. Rainfall and river discharge data

Rainfall over the catchment was obtained from a Global Precipitation Measurement (GPM) Integrated Multi-satellitE Retrievals for GPM (IMERG) product (Huffman et al., 2014). We use the final Level 3 product developed for research applications, which is available daily on a 0.1°×0.1° longitude/latitude grid (https://gpm.nasa.gov/). Rainfall was extracted over the study period (2018-2019) and

averaged in the river catchment area shown in Figure 1b. In order to filter out high frequency variability irrelevant to our study, we used monthly cumulative rainfall.

Historical estimates of the Ouémé River discharge at Bonou (~70 km upstream from the Nokoué Lagoon) and the Sô river discharge at Sô-Awa (~3 km upstream from the lagoon) are available. These daily data, available from the 1950's to the 1990's, were collected by the general Benin Directorate of water and made available by the Système d'Informations Environnementales sur les Ressources en Eau et Modélisation (SIEREM: http://www.hydrosciences.org/spip.php?article1236). A daily climatology was constructed from this multi-year dataset and the Sô and Ouémé discharges were summed to provide an estimate of the total fresh water discharge into the lagoon.

2.4. Time series analyses

The variability of the WL across temporal scales was investigated using a wavelet-based analysis (Torrence and Compo, 1998; Guo et al., 2015). The wavelet power spectrum, that estimates the spectral characteristics of the WL signal as a function of time, is computed here using the Morlet wavelet transform. In order to compare spectral peaks across different scales, the obtained wavelet power spectra, that are slightly biased, are rectified normalizing them by the local scale (Liu et al., 2007; Veleda et al., 2012). Wavelet decomposition can also be used for signal reconstruction and filtering (Torrence and Compo, 1998). By summing over a subset of scales, we here construct WL wavelet-filtered time series in several spectral bands, from high-frequency (periods < 5h) to subtidal and low-frequency (periods > 20 days) variability.

Global power spectra obtained from wavelet analyses provide consistent estimation of the true power spectra computed from Fourier analyses (Percival, 1995). However, due to the width of the wavelet filter in Fourier space, any close peaks in Fourier spectra could be smoothed out by the wavelet analysis, particularly at small (high-frequency) wavelet scales (Hudgins et al., 1993; Torrence and Compo, 1998). Thus, in order to resolve close principal tidal constituents, their mean amplitudes and phases (e.g. Table 1) are obtained from harmonic analyses using T_TIDE package in MATLAB for each time series (Pawlowicz et al., 2002). The temporal evolution of tidal amplitudes is subsequently investigated in the diurnal (D1), semi-diurnal (D2), and quarter-diurnal (D4) spectral bands by integrating wavelet power in these specific frequency/period bands and converting them into wavelet amplitudes as in Guo et al. (2015). The D1, D2

and D4 amplitudes are computed for periods of 15-36h, 7.5-15h and 5-7.5h, respectively.

3. Results

3.1. Low-frequency variations

At the entrance of the Nokoué Lagoon at P_{South}, in the periods from February to August 2018 and from December 2018 to July 2019, the lagoon WL was low at mean WL of 0.5-0.6 m in 2018 and 0.6-0.7 m in 2019 (Figure 2a). These periods coincide with climatological periods when rivers are at baseflow and have discharges of less than ~50 m^3/s (Figure 2b). From 20 August 2018 to 30 September 2018, the mean WL increased to reach a maximum value of ~1.4 m (Figure 2a). The peak observed in 2018 coincides with the maximum climatological river discharges of ~800 m^3/s at the beginning of October. The decrease of the lagoon WL from 1.4 m to less than 0.6 m was observed between early October and early December 2018. The duration of the decrease was comparable to that of the WL rise. In contrast, the duration of increasing/decreasing WL were strongly asymmetric in 2019. The flooding phase began in late July 2019 and took 3 months to reach the maximum of ~1.4 m on 31 October 2019. Although the beginning of the flooding phase in 2019 approximately follows the climatological river discharge, the maximum WL was observed 1 month later than the average peak of the hydrograph. In 2019, the decrease of the lagoon WL took only 1 month, and the low-WL was reached at the beginning of December, as in 2018.

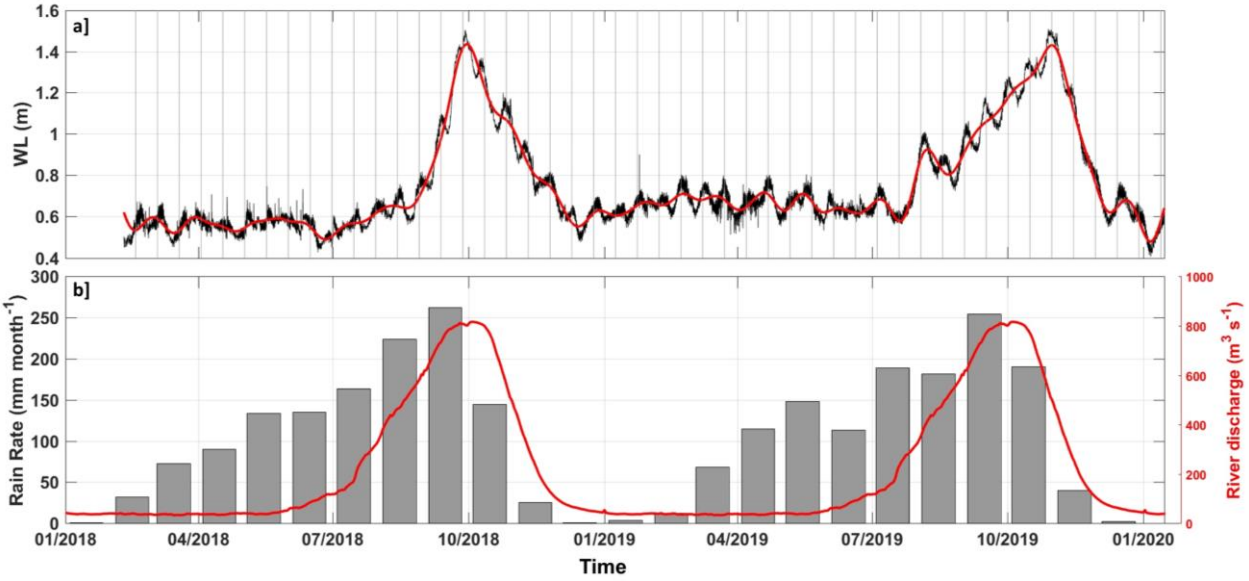

Figure 2. Water-level and hydrological variations. a] Temporal variations of the water-level (WL) at P_{South}; red line shows the low-frequency component associated with periods longer than 20 days where grey vertical lines correspond to the

time of oceanic spring tides. b] Monthly cumulative rainfall over the Ouémé river catchment basin (grey bars) and estimated climatological river discharge (red line).

The monthly cumulative rainfall inferred from satellite data in the Sô and Ouémé catchment basins do not show strong differences between the time periods of the rainy season of 2018 and 2019 (Figure 2b). In both 2018 and 2019, the maximum rainfalls occurred in September. However, October 2019 was 35% rainier (~190 mm) than October 2018 (~140 mm), which explains the 1-month delay observed in 2019 on the maximum WL (Figure 2a). Similarly, heavy rainfalls (~190 mm) observed in July 2019, are responsible for the earlier rise in WL in 2019, as well as for the local maximum elevation of ~0.95 m observed at the beginning of August 2019. Heavy rainfalls in July-August 2019 also contributed to spread out the flooding phase and delay the flood peak in the lagoon.

Low-frequency WL variations of the Nokoué Lagoon are related to the rainfall in the catchment basin and the river flows that discharge fresh water into the lagoon. However, superimposed on these low-frequency fluctuations, Figure 2a shows that the unfiltered WL signal exhibits high-frequency variability patterns. The main goal of the following Sections is thus to investigate these distinct modes of variability.

3.2. WL Wavelet analysis

During the 2-year period, the 4 WL timeseries show similar patterns, not only at low-frequency (Figure 3). Superimposed on the already described low frequency WL variations, higher frequency WL variations with typical ranges of ~±20 cm that decrease from the Cotonou channel to the Nokoué Lagoon are evident (Figure 3). In order to better identify the dominant frequencies, we performed a wavelet analysis (Figures 3 and 4). WL timeseries show time-dependent variability with contributions from distinct frequency bands at certain times. Spectra can be divided into 5 main period bands, from high to low frequencies: i) high-frequency component with periods shorter than 5 hours; ii) tidal component with periods ranging between 5 hours and 1.5 days; iii) subtidal component with periods of 1.5-10 days; iv) fortnightly component with periods of 10–20 days; and v) low-frequency component with periods longer than 20 days.

The low-frequency component has been described in Section 3.1 and corresponds to large WL variations mainly due to rainfall in the catchment basins that

drives the seasonal change in river discharge into the lagoon. In contrast, the subtidal component does not present significant spectral energy (Figures 3 and 4) and is thus not further investigated. Fortnightly, tidal and high-frequency components are described in more detail.

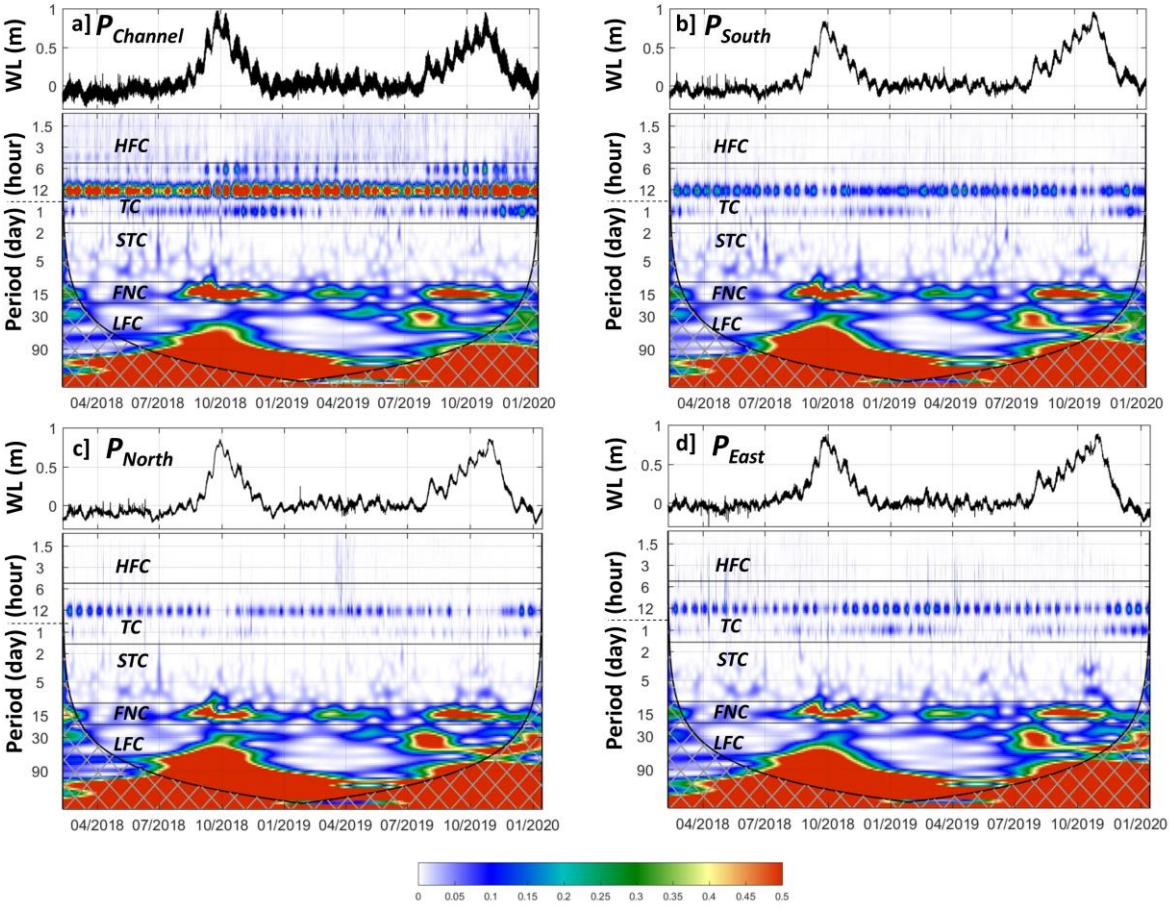

Figure 3. Water-level (WL, in m) timeseries and corresponding rectified continuous wavelet power spectra, at a) $P_{Channel}$, b) P_{South}, c) P_{North}, and d) P_{East}. The rectified wavelet power is $log_2(A^2/s)$, where A is the wavelet coefficient amplitude, and s the scale it associates (Liu et al., 2007). The y axis is on a log_2 scale and in day (hour, respectively) for periods higher (lower) than 1 day. The cone of influence is indicated by hatched area by 95% confidence level due to the edging effects. Horizontal black lines on the wavelet spectra delimit 5 frequency bands: High-frequency component (HFC) (periods<5 hours); Tidal component (TC) (5-36 hours); Subtidal component (STC) (1.5-10 days); Fortnightly component (FNC) (10–20 days); Low-frequency component (LFC) (>20 days).

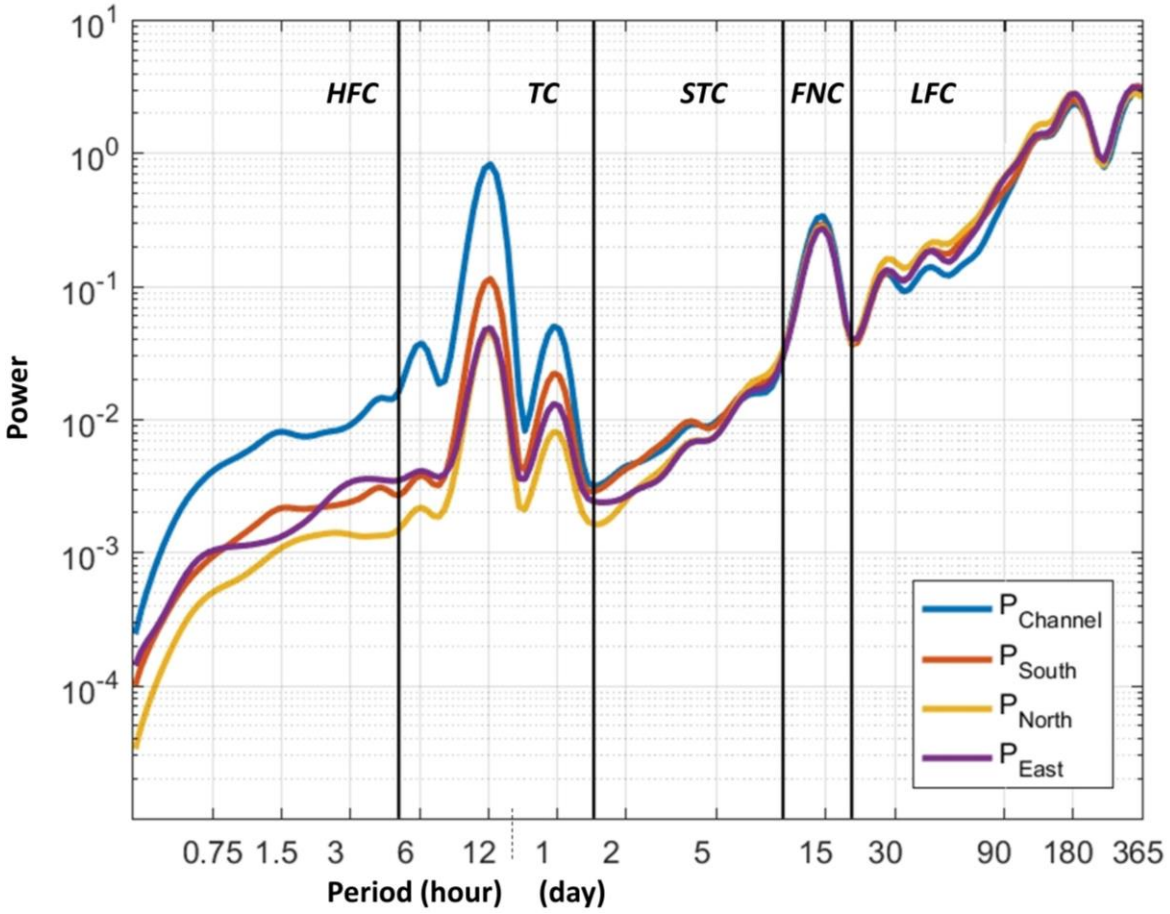

Figure 4. Global wavelet power spectra obtained by averaging over time the wavelet power spectrum at a) $P_{Channel}$, b) P_{South}, c) P_{North}, and d) P_{East}. Vertical black lines delimit the 5 frequency bands detailed in Figure 4.

3.3. Fortnightly and tidal components

a) Harmonic Analysis and main tidal constituents

Figures 3 and 4 show relatively strong spectral energy in the fortnightly (MSf) component. These oscillations of a period of ~14.8 days on the mean WL are associated with neap and spring tides. Indeed, the combination of the principal lunar (M2) and solar (S2) semidiurnal tidal constituents, characterized by very close periods (Table 1), induces a compound tide (MSf) and fortnightly variation of the oceanic semi-diurnal tide amplitude (e.g. LeBlond, 1979; Pugh, 1987). In the open-ocean, where the mean WL variations are weak compared to the tidal range, both the highest and lowest sea-levels are observed during spring tides, and the mean WL is not significantly modulated at MSf frequencies (Table 1). In contrast, in shallow lagoons or estuaries, complex non-linear interactions between oceanic semi-diurnal tides, river fluxes, bottom friction and morphology of the channel, result in MSf variations of the WL (LeBlond, 1979; Gallo and Vinzon, 2005; Guo et al., 2015). These MSf variations are observed in the Cotonou

channel and Nokoué Lagoon (Table 1), where the highest high-waters are observed during spring tides whereas the lowest low-waters are observed during neap tides (Figures 2a and 3). This is due to the fact that the tidal amplitude is generally weaker than the fortnightly variations of the mean WL (Figures 2a and 3; Table 1) induced by tidal-river interaction processes (e.g. LeBlond, 1979; Guo et al., 2015). Harmonic analyses indicate a mean MSf amplitude of ~4 cm (Table 1), which strongly increases to 10-15 cm during the wet season (not shown but see the evolution of the fortnightly component in Figure 3).

In the open-ocean off Cotonou, tides are semi-diurnal with a relatively important diurnal component (Table 1). Semi-diurnal tide constituents (A_{M2}+A_{S2}) are typically of ~70 cm amplitude whereas diurnal constituents (A_{O1}+A_{K1}) are of ~15 cm. As a result, the tidal form factor, $F = \frac{A_{O1}+A_{K1}}{A_{M2}+A_{S2}}$, which is the amplitude ratio of the diurnal to semi-diurnal tide constituents, is of 0.22, close to the mixed-tide threshold of 0.25 (Courtier, 1938). Off Cotonou, the tide is thus of semi-diurnal-dominant type, but characterized by two slightly unequal high and low tides per day. In the Cotonou channel and Nokoué Lagoon, tidal ranges are strongly dampened and the tidal form factor increases to 0.41 (Table 1). This suggests a stronger modulation of the tides at diurnal scale in the lagoon and a stronger attenuation of the semi-diurnal constituents compared to the diurnal constituents.

In shallow water, the progression of a tidal wave is modified by bottom friction and other physical processes that lead to the distortion and asymmetry of the tidal wave (Pugh et al., 1987). These non-linear effects are associated with the generation of higher harmonics such as the main M4 constituent, which is the second harmonic (or overtide) of the principal lunar tide M2, that causes disparities in the rising and falling times (e.g. Pugh et al., 1987; Gallo and Vinzon, 2005; Ray, 2007). Thus, tidal wave deformation and asymmetry are mainly due to M2-M4 interactions (e.g. Friedrichs and Aubrey, 1988; Speer and Aubrey, 1985). The general flood-dominated character of the lagoon system is highlighted by the phase difference of $2\varphi_{M2} - \varphi_{M4}$ in the range of 0-90° that leads to a longer falling tide than rising tide (Friedrichs and Aubrey, 1988; Guo et al., 2015). The magnitude of the amplitude ratio of the M4 and M2 components ($\frac{A_{M4}}{A_{M2}}$) is an indicator of the strength of the tidal asymmetry. This factor is of 0.02 at P_{Ocean} where the tide is

symmetric, but increases to 0.11-0.15 in the lagoon system indicating a stronger asymmetry and, on average, a deformation of the tidal wave (Table 1).

Table 1. Average tidal properties: Tidal amplitudes (A) and phases (φ) of major diurnal (D1), semi-diurnal (D2), quarter-diurnal tides (D4) and fortnightly (FNC) components' frequencies at P_{Ocean}, $P_{Channel}$, P_{South}, P_{North} and P_{East}. These average tidal constituent properties were determined by harmonic analyses of 2-year WL timeseries using T_TIDE (Pawlowicz et al., 2002). Periods are in hours, except for FNC frequencies where they are in days.

			P_{Ocean}		$P_{Channel}$		P_{South}		P_{North}		P_{East}	
		Period	A (cm)	φ (°)	A (cm)	φ (°)	A (cm)	φ (°)	A (cm)	φ (°)	A (cm)	φ (°)
FNC	MSf	14.77	0.0	125	4.2	60	3.9	66	4.0	70	3.9	69
	Mf	13.66	0.0	96	1.6	55	1.3	63	1.4	60	1.3	60
D1	O1	25.82	2.6	318	0.3	119	0.2	159	0.2	177	0.2	181
	P1	24.07	3.8	346	0.4	45	0.2	78	0.1	81	0.1	60
	S1	24.00	0.1	91	1.0	110	1.0	115	0.2	186	0.4	144
	K1	23.93	12.5	1	1.4	35	0.6	89	0.5	115	0.7	112
D2	N2	12.66	10.8	101	1.5	130	0.5	153	0.3	217	0.3	222
	M2	12.42	50.8	105	7.5	134	2.7	156	1.5	221	1.6	232
	S2	12.00	17.8	130	1.8	167	0.6	241	0.7	299	0.6	306
	K2	11.97	4.3	144	0.8	184	0.3	196	0.2	253	0.2	265
D4	M4	6.21	1.3	319	1.1	266	0.3	280	0.2	16	0.2	18
	MS4	6.10	0.0	104	0.7	288	0.2	299	0.1	53	0.1	48

b) Tidal WL fluctuations during dry/wet seasons and spring/neap tides

Figure 5 shows two-day snippets of WL fluctuations during the dry and wet seasons (April and October, respectively) and for different phases of spring-neap tidal cycles. During dry season spring tides (Figure 5a), the maximum tidal amplitude is of ~80-90 cm in the ocean. It decreases to ~10-15 cm in the Cotonou channel and ~3-5 cm in the lagoon. During this period, the average diurnal tidal amplitude (AD1) is of ~15 cm in the offshore ocean and of 1-2.5 cm in the lagoon (Table 2). Similarly, the average semi-diurnal tidal amplitude (AD2) varies from ~90 cm at P_{Ocean} to ~3-15 cm at the other stations (Table 2). The AD1/AD2 ratio is 0.1-0.3, suggesting that the tide is mainly semidiurnal without strong diurnal modulation, as seen in Figure 5a. Both the quarter-diurnal amplitude (AD4) and the AD4/AD2 ratio are weak and the tide appears mostly symmetric, without strong deformation.

During dry season neap tides (Figure 5b), the minimum tidal amplitude is of ~20 cm at P_{Ocean} but is strongly modulated at diurnal scale. The AD1 amplitude is ~18 cm and

AD2 decreased to ~36 cm leading to a relatively strong AD1/AD2 ratio of 0.5 (Table 2). In the lagoon, tidal amplitudes decrease to ~1-2 cm for AD1 and to 2-7 cm for AD2. These values are weaker but the associated AD1/AD2 ratios (0.3-0.7) are slightly higher to what was observed during spring tides (Figure 5a-b and Table 2). In the Cotonou channel and Nokoué Lagoon during dry season, the rising and falling tidal durations are slightly unequal and the tide is only very slightly asymmetric, as indicated by weak AD4 values of 0.1-0.2. Indeed, the ebb-tide lasts ~30-45 mn longer than the flood-tide, hence the lagoon system tends to be flood-dominated (e.g. Speer et al., 1991).

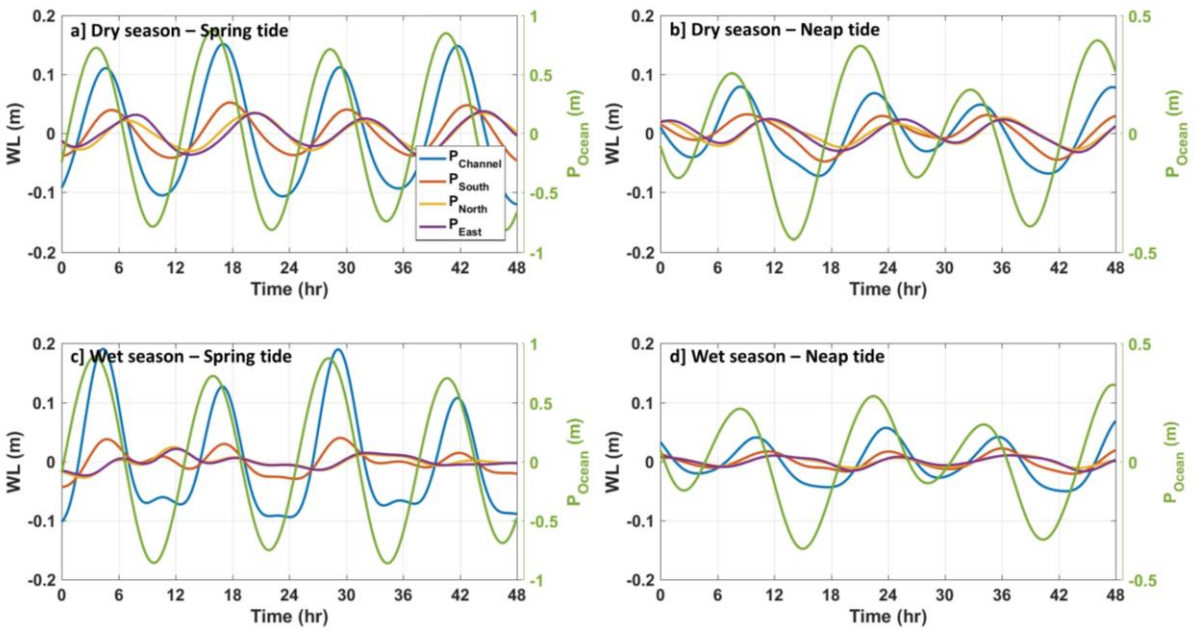

Figure 5. Examples of water-level evolution in the tidal frequency band (periods of 5-36 hr) during a] a dry season spring tide, b] a dry season neap tide, c] a wet season spring tide, d] a wet season neap tide. Water levels (WL, in m) in the Cotonou channel ($P_{Channel}$) and Nokoué Lagoon (P_{South}, P_{North}, P_{East}) correspond to left axes whereas WL in the ocean (P_{Ocean}) correspond to right axes (and green lines).

During the wet season, the tide characteristics in the open ocean are similar to the dry season, with AD1 of ~15 cm and AD2 varying from ~95 cm for spring tides to ~30 cm for neap tides (Figure 5c-d and Table 2). In contrast, tide characteristics are significantly modified in the channel and the lagoon, and more particularly during wet season spring tides (Figure 5c). AD2 decreases during wet season and AD1 tends to increase (see also wavelet power spectra in Figure 3). The tidal form factor AD1/AD2 increases from ~0.1-0.7 during the dry season, to 0.5-2.2 during the wet season (Table 2), as a result of a stronger modulation of the tides at diurnal scale during high water periods. During spring tides (Figure 5c), the flood duration is 4-5 h, whereas the ebb-

tide lasts 7-8 h. Notably the wave shape of the tides tends to be positively skewed with a slack-tide asymmetry, in particular at $P_{Channel}$ (blue line in Figure 5c). This slack-tide asymmetry is due to a phase difference between M2 and M4 ($2\varphi_{M2} - \varphi_{M4}$) that is, on average, close to 0° (Table 1) (e.g. Guo et al., 2019).

Finally, high and low tides are systematically observed 1 hour later at $P_{Channel}$ than at P_{Ocean} (Figure 5). In contrast, the high or low tide phase shift between P_{South} and P_{North} or P_{East}, varies from 1h-3h during dry season (Figure 5a,b) and is strongly uncertain during wet season when the tide is much more asymmetric and deformed (Figure 5c,d). Note also that winds can impact WL in shallow lagoons, in particular by pushing and piling up water in the downwind direction (e.g. Stieglitz et al., 2013; Colvin et al., 2018). However, data from the weather station reveals that the dominant southwest wind is weak and varies from 2.2. m s^{-1} in December to 4.5 m s^{-1} in August. Similarly, at diurnal scale, the wind only varies by 2 m s^{-1}, being minimum at 6-7 am and maximum at 3-4 pm. Considering a steady state balance between the wind-stress and the barotropic pressure gradient generated by the slope of the free surface, these typical winds would result on wind setups of ~1-3 cm in the northeastward direction (see equations in e.g. Colvin et al., 2018). This weak signal could not be evidenced in the WL dataset, and no significant WL slope was observed between P_{North}/P_{East} and P_{South}, neither at seasonal nor diurnal scales. However, as described in the following Section, high-frequency fluctuations of the wind field generate high-frequency variations of the WL slope in Nokoué Lagoon.

Table 2. Average tidal amplitudes of diurnal (AD1), semi-diurnal (AD2), and quarter-diurnal tides (AD4) at P_{Ocean}, $P_{Channel}$, P_{South}, P_{North} and P_{East} and for 4 selected 48-hour periods. Amplitude ratios (AD1/AD2 and AD2/AD4) are also indicated. These average tidal constituent properties were determined by integrating wavelet powers in specific frequency/period bands (15-36h for D1, 7.5-15h for D2, and 5-7.5h for D4). Amplitudes are in cm.

	P_{Ocean}	$P_{Channel}$	P_{South}	P_{North}	P_{East}
			Dry Season – Spring Tide		
AD1	13.3	2.6	0.9	1.0	1.0
AD2	94.2	14.2	5.1	3.4	3.5
AD4	3.8	2.0	0.6	0.3	0.4
AD1/AD2	0.14	0.18	0.17	0.30	0.29
AD4/AD2	0.04	0.14	0.12	0.10	0.11
			Dry Season – Neap Tide		
AD1	17.6	3.1	2.2	0.6	1.1
AD2	36.0	6.7	3.2	2.4	2.7

AD4	1.9	1.2	0.5	0.4	0.3
AD1/AD2	0.49	0.47	0.70	0.26	0.42
AD4/AD2	0.05	0.18	0.15	0.18	0.13
		Wet Season – Spring Tide			
AD1	14.9	3.3	1.8	1.5	1.5
AD2	95.3	14.0	2.7	0.7	0.7
AD4	3.8	5.7	1.5	0.8	0.7
AD1/AD2	0.16	0.24	0.68	2.06	2.24
AD4/AD2	0.04	0.41	0.57	1.02	1.01
		Wet Season – Neap Tide			
AD1	16.6	2.1	0.6	0.5	0.6
AD2	28.0	5.1	1.9	1.0	1.1
AD4	1.7	1.0	0.5	0.2	0.3
AD1/AD2	0.59	0.41	0.34	0.54	0.53
AD4/AD2	0.06	0.21	0.24	0.21	0.28

3.4. High-frequency component (periods < 5 hours)

Relatively strong HF variability was observed between February and June 2018, October-November 2018, and February to June 2019 (Figure 6a). For example, during a 2-week period in 2018, 4 individual HF events were observed (Figure 6b). These high-frequency fluctuations can be either in phase or in opposition between the different stations. Typical oscillations of ±5-10 cm are observed.

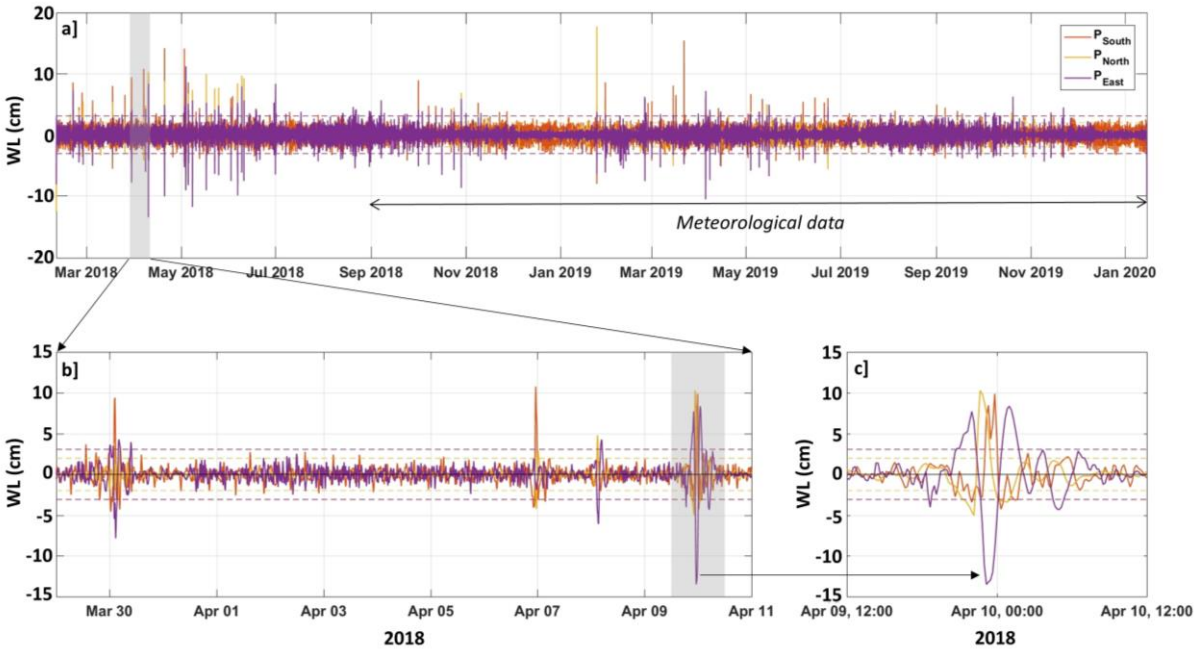

Figure 6. High-frequency component (HFC) of the water level evolution in the Nokoué Lagoon (P_{South}, P_{North}, P_{East}). a] HFC (periods < 5 hours) for the 2-year study period (2018-2019), showing strong high-frequency events. b] HFC for a 12-day period in April 2018. c] zoom for a particular high-frequency event observed in April 10, 2018. In these figures, horizontal dashed lines correspond to ±4 standard deviations around the mean and are used to automatically detect high-frequency events associated with seiches. The period with available meteorological data (September 2018-January 2020) is also indicated by a black arrow in a].

As an example, Figure 6c shows the HF WL variations for the particular event that occurred during the night 09-10 April 2018. Between 08:00 and 10:00 pm, the WL increased by ~7-8 cm in the eastern part of the lagoon (P_{East}) at a simultaneous decrease of 4-5 cm at P_{South} and P_{North}. Thus, this rapid evolution generated a WL difference of 12-13 cm between the East and the central line of the lagoon joining P_{South} and P_{North}. After 10:00 pm, the WL rapidly decreased (increased, respectively) at P_{East} (P_{South} and P_{North}) to reach a maximum negative (positive) anomaly of -13.5 cm (+10 cm) between 11:00 pm and midnight (Figure 6c). This led to a maximum WL difference of ~23 cm between the eastern and central parts of the lagoon. Subsequently, the WL began to oscillate

around its equilibrium value with amplitudes of a few cm. These oscillations, characterized by a period of ~2h45mins, were rapidly dissipated on 10 April after 08:00 am. This ~12-hour duration event, characterized by regular WL free standing-wave oscillations that are progressively dampened, is typical of a seiche event as frequently observed in other lakes, lagoons or coastal embayments (e.g. Chapman and Giese, 2001). For this particular event, the observed standing-wave oscillation period of 2h45mins is in close agreement with the Merian's theoretical period of a seiche oscillation in a rectangular flat-bottom basin (Chapman and Giese, 2001): considering the larger dimension of the Lagoon (L = 20 km) and a mean depth (H) of 1.3 m, the Merian's theoretical period value ($T = \frac{2L}{\sqrt{gH}}$) is of ~3h.

In order to better characterize such HF events, and to provide a more robust description of their main characteristics, a composite analysis was performed. First, individual HF events were filtered as any event associated with a strong WL increase at a given lagoon station (P_{South}, P_{North}, and P_{East}) and a simultaneous strong WL decrease in another gauged station. In order to ensure a high confidence level and exclude any potential false detection, a strong increase/decrease is defined as higher than +/- 4 standard deviations from the mean (Figure 6). Peaks with such high variations occur less than 0.1% of the time. A total of 44 HF events, significantly impacting at least 2 WL stations, were detected. Interestingly, more than 75% (34 on 44) of these events were associated with a strong WL minimum in the eastern part of the lagoon at P_{East}, as also observed in Figure 6c. In terms of seasonality, about 85% of the 44 HF events took place during the dry season between February and June and none of them between August and September.

Second, since the lagoon is elongated in East-West direction and seiche phenomena are expected to more likely develop along the elongated direction, we selected only HF events characterized by a significant WL minimum at P_{East}. Furthermore, after visual inspections, we retained 32 events characterized by similar evolutions in meteorological parameters. Figure 7a displays the composite analysis of the WL evolution for these 32 events, obtained by centering each event at the time the WL minimum at P_{East} was observed (t=0h in Figure 7). On average, about 3 hours before the start of the seiche, the WL gently rises by 2 cm to the East and decreases by ~1 cm at P_{South} and P_{North}. Note that the seiche is triggered at time t=-1.5h, when the WL starts to decrease (increase respectively) at P_{East} (P_{South} and P_{North}). The WL anomaly reaches its

minimum value (-5 cm) at P_{East} at t=0h, while maximum WL anomalies (~2 cm) are observed at P_{North} and P_{South} at t=-0.5h and t=+0.5h respectively. Then, as observed for the individual event shown in Figure 6, the WL oscillates with inverse anomalies between P_{East} and P_{North}/P_{South} (Figure 7a), with an oscillation period of ~3h-3h30. The dissipation is much faster that the single event analyzed in Figure 6, due to the averaging of 32 events that can be characterized by slightly different periods and amplitudes.

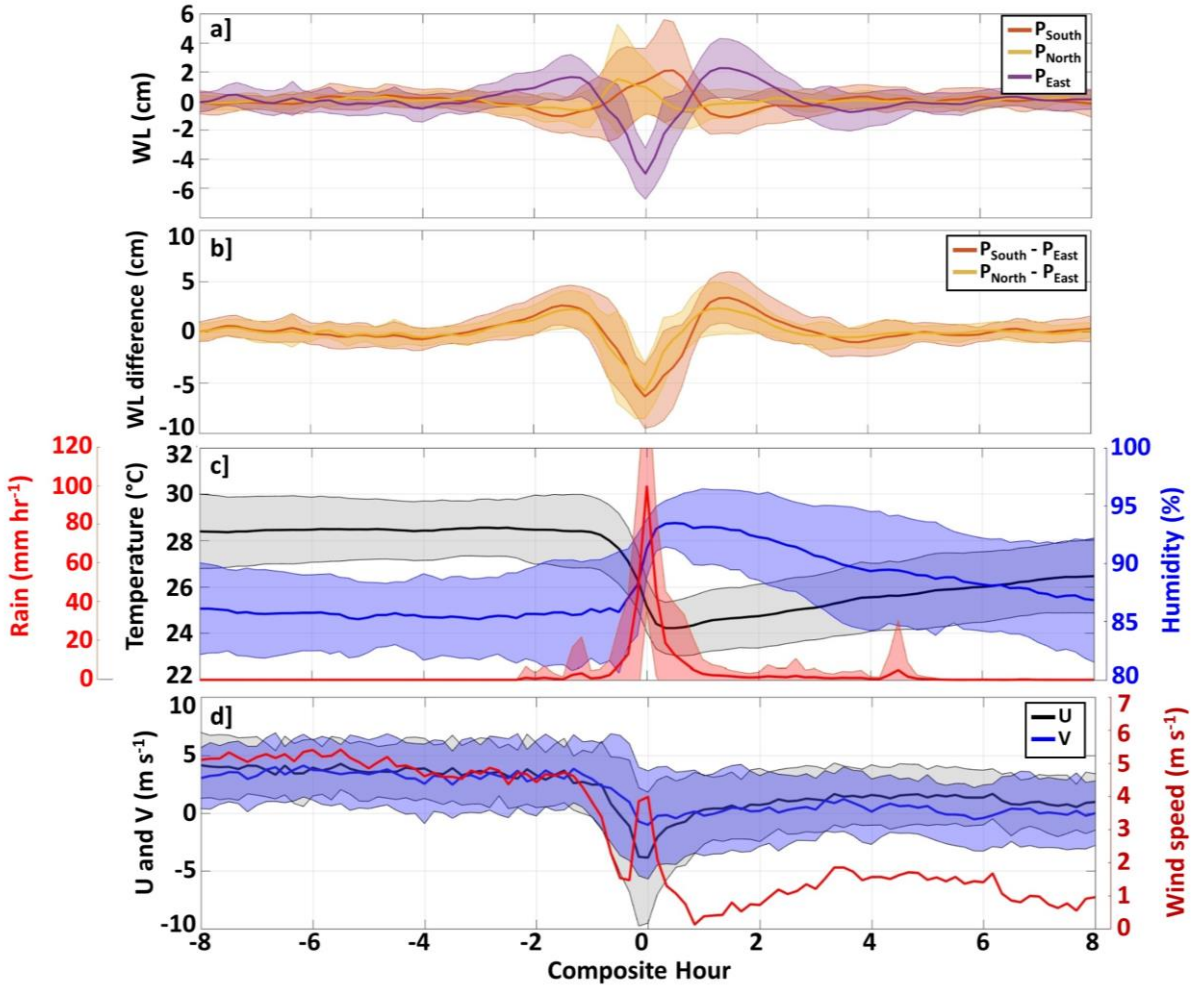

Figure 7. Composite analysis of the high-frequency seiche events and associated atmospheric parameters. a] Averages of water-level (WL, in cm) evolution in the Nokoué Lagoon (P_{South}, P_{North} and P_{East}) for the 32 high-frequency events associated with a maximum negative WL anomaly at P_{East} at t = 0. b] Mean water-level differences between P_{South} and P_{East} and between P_{North} and P_{East}. c] Mean temporal variations of air-temperature (in °C, black line), air-humidity (in %, blue line) and rain (in mm/hr, red line). d] Mean temporal variations of wind velocity components (in black and blue, left axis) and wind speed (in red, right axis). Color shading correspond to ±1 standard deviation around the means. In order not to overload the figure, standard deviations are not shown for wind speed in c].

Finally, in order to better understand the forcing mechanisms involved in the seiche generation, a composite analysis of some key meteorological parameters was

548 performed (Figure 7c-d). Leading up to the seiche triggering, atmospheric conditions are
549 relatively stable with on average an air temperature of ~28.5°C, a humidity of ~85%,
550 and no rain (Figure 7c). The wind is also regular, blowing towards the Northeast (zonal
551 and meridional components are equal and positive) with a mean speed of 4-5 m s^{-1}
552 (Figure 7d). This wind regime tends to accumulate water in the Northeast/East of the
553 lagoon as observed in Figure 7a. At the start of the seiche (t=-1.5h) the wind suddenly
554 decreases and progressively reverses (Figure 7d). At t=0, when the WL is minimum at
555 P_{East}, the wind blows towards the West-Southwest with a mean speed of ~4 m s^{-1} (Figure
556 7d). This strong and rapid wind inversion is thus the main forcing mechanism of the
557 seiche, causing the displacement of the water from the East to the West and initiating
558 the WL oscillations. After this maximum wind inversion, the wind progressively blows
559 again towards the Northeast but with a very weak intensity (< 2 m s^{-1}). Interestingly,
560 during the seiche event the air temperature suddenly drops by 4-5°C, the humidity
561 increases to reach an average value of 93% and very strong rain events are observed
562 (Figure 7c). These showers of up ~100 mm/h rainfall have a duration of 30-60 mn.
563 These patterns are likely related to the passage of fast-moving squall-lines,
564 characterized by strong pressure jumps and downdraft winds, with short but intense
565 rainfalls (e.g. Omotosho, 1984; 1985; Schrage and Fink, 2007). Interestingly, the
566 seasonal variation of the number of squall-lines in West African coastal regions, shows a
567 bi-modal distribution with a strong maximum in March-June and almost no squall-line in
568 July-September (Omotosho, 1984; 1985). Both the number of squall-lines and the
569 number of seiche events show similar seasonal variations (85% of the seiche events
570 were observed in February and June and none in August-September), which strongly
571 suggests that the passage of these atmospheric disturbances (squall-lines) are likely
572 responsible of the observed seiche phenomena.
573

574 ## 4. Discussion

575 As noted by Ekeu-Wei (2018), floods are one of the most devastating natural hazards
576 in West Africa, increasing in frequency, magnitude and impact in recent decades (Aerts et al.,
577 2014; Di Baldassarre et al., 2010). Flood in West-Africa is thus a growing issue and various
578 political or economic capitals are concerned by flooding, in particular due to their proximity
579 from coastal lagoons fed by important watersheds (e.g. Lagos in Nigeria, Cotonou in Benin,
580 Lomé in Togo, Abidjan in Ivory Coast, etc.). Local governments therefore need information

to implement appropriate flood management measures. However, the acquisition and maintenance of environmental and climate observation networks in these developing regions is very challenging despite their vulnerability to climate variability and change (Ampadu et al., 2013; Eku-Wei, 2018 ; Dinku, 2019 ; Brocca et al., 2020). As such, WL timeseries in West-African lagoons are rare or non-existent. Results presented in this study, which are based on several 2-year timeseries of WL in the Nokoué Lagoon in Benin, are therefore unique in West-Africa and provide important information on the hydrological functioning of this coastal lagoon for the future implementation of flood early warning system.

In particular, this study complemented previous limited studies (Le Barbé et al., 1983; Djihouessi and Aina, 2018), highlighting the main roles of river runoffs, tides and winds in the WL variations of Nokoué Lagoon. Observed low-frequency subtidal WL variations of ~0.8-0.9 m are the result of the importance of continental water inflow and the lagoon's evacuation capacities, which depend on the ocean level. At regional scale, the WL has only been measured in the Ebrié Lagoon (Ivory Coast) for 1-year in 1952. This lagoon also showed an increase of 50 cm during watershed flooding in October-November (Varlet, 1978; Durand and Guiral, 1994). In Nokoué Lagoon, our results suggested a 1-month delay between maximum rainfall in the catchment basin and the maximum WL in the lagoon, which is encouraging to elaborate an operational seasonal flood forecasting system in the lagoon from rainfall observations.

Our study also suggests that such forecasting system has to take into account tide forcing. The interaction of M2 and S2 tidal constituents through non-linear bottom friction and river interaction resulted in a pronounced fortnightly-period oscillation of lagoon WL, as expected from one-dimensional simplified models (e.g. Hill, 1994; MacMahan et al., 2014). Tides are strongly attenuated, with a main semidiurnal (M2+S2) tidal amplitude decreasing from 30-90 cm in the ocean to ~1-3 cm in the Nokoué Lagoon (see Table 2 and also Zandagba et al., 2016). The tidal signal is thus altered by the frictional channel that acts as a dynamic low-pass filter (Kjerfve and Magill, 1989) and the Nokoué Lagoon can be classified as a choked coastal lagoon (Kjerfve, 1986) with a choking coefficient varying with the season and ocean tide amplitude (Table 3).

Based on Stigebrandt (1980), many studies have explained choking conditions using a simple one-dimensional model (e.g. Rydberg and Wickbom, 1996), where the response of the WL within the lagoon (η_{lagoon}) to the ocean sea-level forcing (η_{ocean} and M2 tide) and a variable freshwater supply (Q_{river}) is given by:

$$\frac{d\eta_{lagoon}}{dt} = P\frac{\eta_{ocean}-\eta_{lagoon}}{\sqrt{|\eta_{ocean}-\eta_{lagoon}|}} + S \qquad (1)$$

where the parameters characterizing the choking conditions are (Stigebrandt, 1980)

$$P = \frac{hl}{A\sqrt{1+\lambda}}\sqrt{\frac{2gT^2}{a_{ocean}}} \qquad \lambda = 2\kappa\frac{L}{h} \qquad \text{and} \qquad S = \frac{Q_{river}T}{Aa_{ocean}}$$

with g = 9.81 m/s^2 is the gravitational acceleration; T = 12.42 hours and a_{ocean} = 0.5 m, are the M2 tidal period and amplitude in the ocean, respectively; κ ~ 0.003 is a friction coefficient used in quadratic friction laws (e.g. Robinson et al., 1983; Stigebrandt and Molvær, 1988; Sternberg, 1968; Rydberg and Wickbom, 1996); A = 170 km^2 is the lagoon area, L = 4000 m the length of the Cotonou channel, l = 280 m its breadth, and h = 3 m its depth. The river discharge, Q_{river}, is poorly known but estimated climatologies show it varies from ~50 m^3 s^{-1} in low-water season to ~800 m^3 s^{-1} during flood period (Figure 2).

Table 3. Tidal choking coefficients (in bold) obtained from average semidiurnal tidal amplitudes observed in the ocean (a_{ocean}) and Nokoué Lagoon (a_{lagoon}), and from theoretical results from Equation 1 (Stigebrandt, 1980) for different hydrological periods (dry and wet seasons) and tidal characteristics (spring and neap tides). a_{lagoon} was obtained from Table 2, averaging semidiurnal tidal amplitudes (AD2) at the 3 stations located in Nokoué Lagoon (P_{South}, P_{North}, P_{East}).

	Observations			*Theoretical (Stigebrandt, 1980)*		
	a_{ocean} *(cm)*	a_{lagoon} *(cm)*	$C_c = \frac{a_{lagoon}}{a_{ocean}}$	C_C	P	S
			Dry Season (Q_{river} = 50 m³ s⁻¹)			
Spring Tide	94.2	4.0	**0.04**	**0.06**	0.34	0.01
Neap Tide	36.0	2.8	**0.08**	**0.09**	0.54	0.04
			Wet Season (Q_{river} = 800 m³ s⁻¹)			
Spring Tide	95.3	1.4	**0.01**	**0.02**	0.33	0.22
Neap Tide	28.0	1.3	**0.05**	**0.06**	0.62	0.75

In this model, tidal choking depends at first order upon the geometrical characteristics of the lagoon and channel including friction effects (e.g. Stigebrandt, 1980; Hill, 1994; MacMahan et al., 2014). River outflows plays an additional role in modifying both the mean lagoon WL and the tidal amplitude and phase (Stigebrandt, 1980). Given the lagoon and river discharge characteristics, we obtain λ ~ 8 indicating a strong control of tidal choking by bottom friction. P varies from 0.3 for spring semidiurnal tides to 0.6 for neap tides (Table 3). Interestingly, because of extreme hydrological variability, S varies from 0.01 in dry season to 0.8 in wet season (Table 3), implying a strong influence of river discharge for the choking process. Following Stigebrandt (1980; see his Table 1), the predicted choking coefficient

varies from 0.02 to 0.09 (Table 3). These results only slightly differ from our estimates (Table 3), in particular because river inflow is poorly known. This good agreement shows that this simple model is able to explain the observed choking conditions and its strong seasonal and fortnightly variability.

Also, for the considered river outflows (50 and 800 m^3 s^{-1}) the Stigebrandt's (1980) theory predicts a similar tidal asymmetry in the lagoon, with an ebb duration ~35 mn longer than the flood. This is in agreement with what we observed during dry season (30-45 mn), but the observed ebb-flood asymmetry was stronger during flood period. The expected phase delay between high water in the ocean and in the lagoon is predicted to be of 1.5-3 hours (longer phase shifts for stronger river outflows), in agreement with the values observed in Section 3.3b. Furthermore, Stigebrandt (1980) suggested from his theory that the mean WL in the lagoon would increase by 5 cm in low-water period and ~80 cm during flood season, which is very close to our observations (Figure 2). These comparisons between observed and predicted values from the Stigebrandt's (1980) theory at different timescales are very promising for using this simplified one-dimensional models to predict WL in Nokoué Lagoon from river discharge data and tidal constituents. Implementing a forecasting system was beyond the scope of the present study, but this problem and approach will deserve future studies.

Finally, as shown in Section 3.4, the HF WL acquisition rates allowed us to highlight the occurrence of seiches in Nokoué Lagoon and to provide their main characteristics. These HF events, forced by the passage of fast-moving squall lines, are characterized by typical WL oscillations of ±5-10 cm. Seiches are commonly observed in large lakes or lagoon in the World (e.g. Chapman and Giese, 20021). However, due to the lack of continuous WL monitoring, these HF events have been only marginally documented in some lakes of Central and East Africa (e.g. Beauchamp, 1939; 1953; Jollyman, 1955; Fish, 1957; Ward, 1959). In West-Africa, only Varlet (1978) mentioned the occasional existence of damped oscillations in the Ebrié Lagoon whose amplitude could reach 10 cm and whose period was about thirty minutes. He also noted that in 1952, a tornado produced a momentary rise of 5-15 cm in the Ebrié lagoon. Our study, based on a robust statistical analysis, provides an unprecedented description of the seiche phenomenon in an African coastal lagoon. These results provide useful metrics to validate barotropic shallow-water models, that in turn could be used to better understand seiche dynamics in Nokoué Lagoon. They also suggest that, to be exhaustive, flood forecasting system should incorporate or parameterize seiche oscillations in Nokoué Lagoon.

5. Conclusion

The lagoon WL exhibits strong variability in 4 main frequency bands. First, a low-frequency variability is directly associated with the seasonal variation of rainfall and river discharge that causes the WL in the lagoon to increase by 0.9 m between low and high water periods. Some interannual variability was observed, related to variations of rainfall over the watershed and associated river discharge, but the lack of available contemporary hydrological and meteorological data prevents any further diagnostics.

Second, we documented the propagation and interaction of oceanic tidal constituents within the Cotonou channel and Nokoué Lagoon. Fortnightly frequency variations of the mean WL are observed in the lagoon with the highest high-waters observed during spring tides and the lowest low-waters during neap tides. Amplitudes of the fortnightly variations are much higher (10-15 cm) during the wet season. A strong attenuation of the tidal range within the Cotonou channel is observed, as well as the general flood-dominated character of the lagoon. On average, semi-diurnal (diurnal, respectively) tidal amplitudes decreases from ~70 cm (15 cm) in the ocean to ~2-3 cm (<2 cm) within the lagoon. Thus, the relatively long Cotonou channel, that connects the Nokoué Lagoon to the ocean, acts as a natural low-pass filter that reduces tidal effect in the lagoon but increase the fortnightly component, and more particularly during wet season when river discharge is high.

Third, we observed higher frequency WL variability, characterized by periods shorter than 5 h. Most of these energetic events are observed during the dry season, and are associated with typical WL variations of 5-10 cm. These HF patterns correspond to wind-forced seiches associated with the passage of fast-moving squall-lines. The perturbation of the persistent southwest winds by the passage of these atmospheric disturbances leads to the development of seiches with a period of ~3 h. During these events, that are rapidly dissipated, heavy rainfalls are observed and the air temperature drops on average by 5°C.

The observations and diagnostics of this study contribute to a better understanding of the dynamics of the Nokoué Lagoon and may be used to inform an improved management of flood risks of the adjacent low-lying coastal cities. Indeed, our study shows that in order to be realistic, a flood early warning system should not only consider the hydrological regime of the Sô and Ouémé rivers, but also the propagation

and non-linear interactions of the ocean tide that produces significant WL fluctuations of Nokoué Lagoon, in particular at fortnightly periods during flood season (Figures 2-3). In a second step, this flood warning system should also include seiches that give rise to high frequency WL oscillations and can cause additional surges.

Acknowledgments.

Field campaigns and instrumentation were supported by IRD, IRHOB and ANR @RAction chair medLOC (ANR-14-ACHN-0007-01–T.Stieglitz). V. OKPEITCHA was funded by OmiDelta project of the Embassy of the Netherlands in Benin, through a scholarship grant of the National Institute of Water (INE). This work is a contribution to the « JEAI SAFUME » project funded by IRD. Special thanks to the members and crew participating to the deployment and recovery of the sensors, and in particular to Joseph AZANKPO.

References.

Adandedjan, D., Makponse, E., Hinvi, L.C., Lalèyè. P., 2017. Données préliminaires sur la diversité du zooplancton du lac Nokoué (Sud-Bénin). Journal of Applied Biosciences 115, 11476–11489.

Adite, A., and Winemiller, K.O., 1997. Trophic ecology and ecomorphology of fish assemblages in coastal lakes of Benin, West Africa. Écoscience 4 (1), 6-23.

Adite, A., ImorouToko,I., Gbankoto, A., 2013. Fish Assemblages in the Degraded Mangrove Ecosystems of the Coastal Zone, Benin, West Africa: Implications for Ecosystem Restoration and Resources Conservation. Journal of Environmental Protection 4 (12), 1461-1475.

Adjahouinou, D.C., Liady, N.D., Fiogbe, E.D., 2012. Diversité phytoplanctonique et niveau de pollution des eaux du collecteur de Dantokpa (Cotonou-Bénin), Int. J. Biol. Chem. Sci. 6 (5), 1938-1949.

Adjahouinou, D.C., Yehouenou, B., Fiogbe, E.D., Liady, M.N.D., 2014. Caractérisation bactériologique des eaux résiduaires brutes de la ville de Cotonou (Benin). Journal of Applied Biosciences 78, 6705 – 6713.

Aerts, J. C., Botzen, W. W., Emanuel, K., Lin, N., De Moel, H., Michel-Kerjan, E. O., 2014. Evaluating flood resilience strategies for coastal megacities. Science, 344(6183), 473-475.

Ahouangan, M.B.D., Djaby, B., Ozer, P., Hountondji, Y.C., Thiry, A., De Longueville, F., 2014. Adaptation et résilience des populations rurales face aux catastrophes naturelles en Afrique subsaharienne. Cas des inondations de 2010 dans la commune de Zagnanado, Bénin. In: Ballouche, A. & Taïbi, N. A. (Eds.), Eau, milieux et aménagement. Une recherche au service des territoires. Presses de l'Université d'Angers, Angers, France, pp. 265-278.

Ahokpossi, Y., 2018. Analysis of the rainfall variability and change in the Republic of Benin (West Africa), Hydrological Sciences Journal 63 (15-16), 2097-2123.

Aina, M. P., Degila, H., Chikou, A., Adjahatode, F., Matejka, G., 2012a. Risk of intoxication by heavy metals (Pb, Cd, Cu, Hg) connected to the consumption of some halieutic species in lake Nokoué: case of the Penaus schrimps and the Sarotherodon Melanotheron. British Journal of Science 5 (1), 104-118.

753 Aina, M.P., Djihouessi, B., Vissin E.W., Kpondjo, N.M., Gbèdo, V., Sohounhloué K.C.D.,
754 2012b. Characterization of the domestic wastewaters and dimensionality of a pilot
755 treatment station by lagooning at Abomey Calavi city- Benin. J. Engineering Sci. 1 (1),
756 45-50.
757 Allersma, E., Tilmans, W.M.K., 1993. Coastal Conditions in West Africa: A Review. Ocean
758 and Coastal Management 19, 199-240.
759 Ampadu, B., Chappell, N. A., Kasei, R. A., 2013. Rainfall-Riverflow modelling approaches:
760 making a choice of data-based mechanistic modelling approach for data limited
761 catchments: A review. Canadian Journal of Pure and Applied Sciences, 7(3), 2571-
762 2580.
763 Aubrey, D.G., Speer, P.E., 1985. A study of non-linear tidal propagation in shallow
764 inlet/estuarine systems Part I: Observations. Estuarine Coastal Shelf Science 21, 185–
765 205.
766 Beauchamp, R.S.A., 1939. Hydrology of Lake Tanganyika. Int. Rev. ges. Hydrobiol. 39,
767 316-353.
768 Beauchamp, R.S.A., 1953. Hydrological data from Lake Nyasa. J. Ecol. 41, 226-239.
769 Biao, E. I., 2017. Assessing the impacts of climate change on river discharge dynamics in
770 Ouémé river basin (Benin, West Africa). Hydrology 4 (47).
771 Brocca, L., Massari, C., Pellarin, T., Filippucci, P., Ciabatta, L., Camici, S., Kerr, Y.H.,
772 Fernández-Prieto, D., 2020. River flow prediction in data scarce regions: soil moisture
773 integrated satellite rainfall products outperform rain gauge observations in West
774 Africa. Scientific Reports, 10(1), 1-14.

775 Brookes, J., Povilanskas, R., Khokhlov, V., 2018. Assessing, quantifying and valuing the
776 ecosystem services of coastal lagoons. Journal for Nature Conservation 44, 50-65.

777 Carrere L., Lyard, F., Cancet, M., Guillot, A., Picot, N., 2016. FES 2014, a new tidal model -
778 Validation results and perspectives for improvements, presentation to ESA Living
779 Planet Conference, Prague 2016.

780 Chapman, D. C., Giese, G.S., 2001. Waves: Seiches, in Encyclopedia of Ocean Sciences 5,
781 edited by J. H. Steele, K. K. Turekian, and S. A. Thorpe, pp. 2724–2731, Academic,
782 London.

783 Choplin, A., 2019. Produire la ville en Afrique de l'Ouest : le corridor urbain de Accra à
784 Lagos. L'Information géographique 83 (2), 85–103.

785 Colleuil B. (1987). Le complexe lagunaire du Lac Nokoué et de la lagune de Porto-Novo
786 (Bénin). In : Burgis M.J. (ed.), Symoens J.J. (ed.), Gac Jean-Yves (coord.). African
787 wetlands and shallow water, Paris : ORSTOM, (211), 188-196.

788 Colvin, J., Lazarus, S., Splitt, M., Weaver, R., and Taeb, P. 2018. Wind driven setup in east
789 central Florida's Indian River Lagoon: Forcings and parameterizations. Estuarine,
790 Coastal and Shelf Science, 213, 40-48.

791 Courtier, A., 1938. Marées. Service Hydrographique de la Marine, Paris, available at :
792 https://journals.lib.unb.ca/index.php/ihr/article/download/27428/1882520184
793 (last access: 24 December 2020).

794 Di Baldassarre, G., Montanari, A., Lins, H., Koutsoyiannis, D., Brandimarte, L., Blöschl, G.,
795 2010. Flood fatalities in Africa: from diagnosis to mitigation. Geophysical Research
796 Letters, 37(22).

797 Dinku, T., 2019. Challenges with availability and quality of climate data in Africa. In
798 Extreme hydrology and climate variability. Elsevier. 71-80.

799 Djihouessi, M.B., Aina, M.P., Kpanou, B.V., Kpondjo, N., 2017. Measuring the Total
800 Economic Value of Traditional Sand Dredging in the Coastal Lagoon Complex of
801 Grand-Nokoue (Benin). Journal of Environmental Protection 8, 1605-1621.
802 Djihouessi, M.B., Aina, M.P., 2018. A review of hydrodynamics and water quality of Lake
803 Nokoué: current state of knowledge and prospects for further research. Reg. Stud.
804 Mar. Sci. 18, 57–67.
805 Djihouessi, M.B., Djihouessi, M.B., Aina, M.P., 2019. A review of habitat and biodiversity
806 research in Lake Nokoué, Benin Republic: Current state of knowledge and prospects
807 for further research. Ecohydrology and Hydrobiology 181, 1-15.
808 Duck, R. W., da Silva, J. F., 2012. Coastal lagoons and their evolution: a
809 hydromorphological perspective. Estuarine, Coastal and Shelf Science 110, 2-14.
810 Durand, J. R., Guiral, D., 1994. Hydroclimat et hydrochimie. In : Environnement et
811 ressources aquatiques de Côtes d'Ivoire. Tome 2 : les milieux lagunaires, Durand J. R.,
812 Dufour P., Guiral D. et Zabi S. G. F. éditeurs. Editions de l'ORSTOM, Paris, 59-90.
813 Ekeu-Wei, I. T. (2018). Evaluation of hydrological data collection challenges and flood
814 estimation uncertainties in Nigeria. Environment and Natural Resources Research,
815 8(2), 44-54.

816 Evtimova, V. V., Donohue, I., 2016. Water-level fluctuations regulate the structure and
817 functioning of natural lakes. Freshwater Biology 61, 251–264.
818 Fish, G.R.,1957. A Seiche Movement and Its Effect on the Hydrology of Lake Victoria.
819 Fish. Publs Colon. Office, London 10, 1-68.
820 Friedrichs, C.T., Aubrey, D.G., 1988. Non-linear tidal distortion in shallow well-mixed
821 estuaries: a synthesis. Estuarine, Coastal and Shelf Science 27 (5), 521-545.
822 Gallo, M.N., Vinzon, S.B., 2005. Generation of overtides and compound tides in Amazon
823 estuary. Ocean Dynamics 55, 441–448.
824 Glenne, B., Simensen, T., 1963. Tidal current choking in the landlocked fjord of
825 NordÅsyatnet. Sarsia, 11(1), 43-73.
826 Gnohossou, P. M., 2006. La faune benthique d'une lagune ouest Africaine (le lac Nokoue
827 au Bénin), diversite, abondance, variations temporelles et spatiales, place dans la
828 chaine trophique. Doctorat, Institut National Polytechnique de Toulouse, France, 184
829 p.
830 Gu, G., Adler, R.F, 2004. Seasonal evolution and variability associated with the West
831 African monsoon system. Journal of Climate 17, 3364– 3377.
832 Guo, L., van der Wegen, M., Jay, D.A., Matte, P., Wang, Z.B., Roelvink, D., He, Q., 2015.
833 River-tide dynamics: Exploration of nonstationary and nonlinear tidal behavior in the
834 Yangtze River estuary. Journal of Geophyical Research Oceans 120, 3499–3521.
835 Guo, L., Wang, Z. B., Townend, I., He, Q., 2019. Quantification of tidal asymmetry and its
836 nonstationary variations. Journal of Geophysical Research: Oceans 124, 773–787.
837 Guragai, B., Hashimoto, T., Oguma, K., Takizawa, S., 2018. Data logger-based
838 measurement of household water consumption and micro-component analysis of an
839 intermittent water supply system. Journal of Cleaner Production 197 (1), 1159-1168.
840 Hill, A.E., 1994. Fortnightly tides in a lagoon with variable choking. Estuar. Coast. Shelf
841 Sci. 38, 423-434.
842 Houéménou, H., Tweed, S., Dobigny, G., Babic, M., Mama, D., Alassane, A., Silmer, R., Ruy,
843 S., Chaigneau, A., Socohou, A., Dossou, H.-J., Badoum, S., Leblanc, M., 2020. Degradation
844 of groundwater quality in expanding cities in West Africa. A case study of the
845 unregulated shallow aquifer in Cotonou. Journal of Hydrology 582, 124438.
846 Hudgins, L., C. A. Friehe, and M. E. Mayer, 1993. Wavelet transforms and atmospheric
847 turbulence. Phys. Rev. Lett., 71, 3279–3282.

Huffman, G.J., Bolvin, D.T., Braithwaite, D., Hsu, K., Joyce, R., Xie, P., 2014. NASA Global Precipitation Measurement (GPM) Integrated Multi-Satellite Retrievals for GPM (IMERG) algorithm theoretical basis Doc., version 4.4. NASA GSFC, 30 pp.

Jollyman, W.H., 1955. Tides and seiches in lake Nyasa. The Nyasaland Journal, Vol. 8, No. 2, 31-35

Kjerfve, B., 1986. Comparative oceanography of coastal lagoons. In: Wolfe DA (ed) Estuarine Variability. Academic Press, New York, pp 63–81.

Kjerfve, B., Magill, K. E., 1989. Geographic and hydrodynamic characteristics of shallow coastal lagoons. Marine geology, 88(3-4), 187-199.

Knoppers, B., 1994. Aquatic primary production in coastal lagoons. In Kjerfve, B. (Ed.). Coastal lagoon processes. Amsterdam, The Netherlands: Elsevier. Elsevier Oceanography Series 60, 243-285.

Lalèyè, P., Philippart, J.C., Poncin, P., 1995. Biologie de la reproduction de deux espèces de Chrysichthys (Siluriformes, Bagridae) du lac Nokoue et de la lagune de Porto-Novo au Bénin. Journal of African Zoology 109 (3), 213-224.

Lalèyè, P., Niyonkuru, C., Moreau, J., Teugels, G.G., 2003. Spatial and Seasonal Distribution of the Ichthyofauna of Lake Nokoué, Benin, West Africa. African Journal of Aquatic Sciences, 28, 151-161.

Lalèyè, P., Villanueva, M.C., Entsua-Mensah, M., Moreau, J., 2007. A review of the aquatic living resources in Gulf of Guinea lagoons with particular emphasis on fisheries management. Journal of Afrotropical Zoology. Proceedings of the Third International Conference on Africa Fish and Fisheries, Cotonou, Benin, 10–14 November 2003, Special issue, 123–136.

Lawin, A.E., Hounguè, R., N'Tcha M'Po, Y., Hounguè, N.R., Attogouinon, A., Afouda, A.A., 2019. Mid-Century Climate Change Impacts on Ouémé River Discharge at Bonou Outlet (Benin). Hydrology, 6 (72), https://doi.org/10.3390/hydrology6030072

Le Barbé, L., Alé, G., Millet, B., Texier, H., Borel, Y., Gualde, R., 1993. Les ressources en eaux superficielles de la République du Bénin. ORSTOM, Paris, 540 pp.

LeBlond, P. H., 1979. Forced fortnightly tides in shallow rivers. Atmosphere-Ocean, 17:3, 253-264, doi: 10.1080/07055900.1979.964906

Liu, Y., San Liang, X., Weisberg, R. H., 2007. Rectification of the Bias in the Wavelet Power Spectrum. Journal of Atmospheric and Oceanic Technology 24 (12), 2093-2102.

880 Lobo, M.T.M.P.S., de Souza Nogueira, I., Fabris Sgarbi, L., Nunes Kraus, C., de Oliveira
881 Bomfim, E., Garnier, J., da Motta Marques, D., Bonnet, M.-P., 2018. Morphology-based
882 functional groups as the best tool to characterize shallow lake-dwelling
883 phytoplankton on an Amazonian floodplain. Ecol. Indic. 95, 579–588.
884 Lyard F., L. Carrere, M. Cancet, A. Guillot, N. Picot, 2021. FES2014, a new finite elements
885 tidal model for global ocean, in preparation, to be submitted to Ocean Sciences-
886 Special issue on Tides.
887 MacMahan, J., van de Kreeke, J., Reniers, A., Elgar, S., Raubenheimer, B., Thornton, E.,
888 Weltmer, M., Rynne, P., Brown, J., 2014. Fortnightly tides and subtidal motions in a
889 choked inlet. Estuarine, Coastal and Shelf Science, 150, 325-331.
890 Mama, D., Deluchat, V., Bowen, J., Chouti, W., Yao, B., Gnon, B., Baudu, M., 2011.
891 Caractérisation d'un Système Lagunaire en Zone Tropicale: Cas du lac Nokoué
892 (Bénin). Eur. J. Sci. Res. 56 (4), 516–528.
893 Newton, A., Brito, A.C., Icely, J.D., Derolez, V., Clara, I., Angus, S., Schernewski, G., Inácio,
894 M., Lillebø, A.I., Sousa, A.I., Béjaoui, B., Solidoro, C., Tosic, M., Cañedo-Argüelles, M.,
895 Yamamuro, M., Reizopoulou, S., Tseng, H.-C., Canu, D., Roselli, L., Maanan, M., Cristina,
896 S., Ruiz-Fernández, A.C., de Lima, R.F., Kjerfve, B., Rubio-Cisneros, N., Pérez-Ruzafa, A.,
897 Marcos, C., Pastres, R., Pranovi, F., Snoussi, M., Turpie, J., Tuchkovenko, Y., Dyack, B.,
898 2018. Assessing, quantifying and valuing the ecosystem services of coastal lagoons.
899 Journal for Nature Conservation 44, 50-65.
900 N'Tcha M'Po, Y., Lawin, E., Yao, B., Oyerinde, G., Attogouinon, A., Afouda, A., 2017.
901 Decreasing Past and Mid-Century Rainfall Indices over the Ouémé River Basin, Benin
902 (West Africa). Climate 5 (74).
903 Odountan, O., de Bisthoven, L.J., Koudenoukpo, C., Abou, T., 2019. Spatio-temporal
904 variation of environmental variables and aquatic macroinvertebrate assemblages in
905 Lake Nokoué, a RAMSAR site of Benin. African Journal of Aquatic Science 44 (3), 219–
906 231.
907 Okpeitcha, V., Chaigneau, A., Morel, Y., Stieglitz, T., Pomalegni, Y., Sohou, Z., Mama, D..
908 Seasonal and interannual variability of salinity in a large West-African lagoon
909 (Nokoué Lagoon, Benin). Submitted to Estuarine Coastal and Shelf Science.
910 Omotosho, J.B., 1984. Spatial and seasonal variations of line squalls over West Africa.
911 Arch. Meteorol. Geophys. Bioklimatol. A. 33, 143 – 150.

912 Omotosho, J.B., 1985. The separate contributions of squall lines, thunderstorms and the
913 monsoon to the total rainfall in Nigeria, J. Clim. 5, 543 – 552.
914 Percival, D. P., 1995. On estimation of the wavelet variance. Biometrika, 82, 619–631.
915 Pawlowicz, R., Beardsley, B., Lentz, S., 2002. Classical tidal harmonic analysis including
916 error estimates in MATLAB using T_TIDE. Comput. Geosci. 28, 929–937.
917 Principaud, J.-M., 1995. La pêche en milieu lagunaire dans le sud-est du Bénin. L'exemple
918 de l'exploitation des acadjas (en danger) sur le lac Nokoué et la basse Sô. In: Cahiers
919 d'outre-mer, 192, 48e année. Togo-Bénin, 519-546.
920 Pugh, D.T., 1987. Tides, Surges and Mean Sea Level. John Wiley and Sons, New York. 472
921 pp.
922 Ray, R. D., 2007. Propagation of the overtide M4 through the deep Atlantic Ocean.
923 Geophyical Research Letters, 34, L21602, doi:10.1029/ 2007GL031618.
924 Robinson, I.S., Warren, L., Longbottom, J.F., 1983. Sea-level fluctuations in the Fleet, an
925 English tidal lagoon. Estuar. Coast. Shelf Sci. 16, 651-668.
926 Rydberg, L., Wickbom, L., 1996. Tidal-choking and bed friction in Negombo Lagoon, Sri
927 Lanka. Estuaries 19e3, 540-547.
928 Schrage, J.M., Fink, A.H., 2007. Use of a rain gauge network to infer the influence of
929 environmental factors on the propagation of quasi-linear convective systems in West
930 Africa. Weather and Forecasting 22, 1016–1030.
931 Speer, P.E., Aubrey, D.G., Friedrichs, C.T., 1991. Non-linear hydrodynamics of shallow
932 tidal inlet/bay systems. In Tidal Hydrodynamics, edited by B. B. Parker, pp. 321–339,
933 John Wiley, Toronto, Canada.
934 Sternberg, R. W., 1968. Friction factors in tidal channels with different bed roughness.
935 Marine Geology 6, 243-260.
936 Stević, F, Mihaljević, M, Špoljarić, D. 2013. Changes of phytoplankton functional groups
937 in a floodplain lake associated with hydrological perturbations. Hydrobiologia 709,
938 143– 158.
939 Stieglitz, T. C., van Beek, P., Souhaut, M., and Cook, P. G. 2013. Karstic groundwater
940 discharge and seawater recirculation through sediments in shallow coastal
941 Mediterranean lagoons, determined from water, salt and radon budgets. Marine
942 Chemistry, 156, 73-84.
943 Stigebrant, A., 1980. Some aspects of tidal interactions with fjord constrictions. Estuar.
944 Coast. Shelf Sci. 11, 151-166.

945 Stigebrandt, A., & Molvær, J. (1988). On the water exchange of Framvaren. Marine
946 Chemistry, 23(3-4), 219-228.
947 Sultan, B., and Janicot, S. 2000: Abrupt shift of the ITCZ over West Africa and intra-
948 seasonal variability. Geophys. Res. Lett. 27, 3353–3356.
949 Texier, H., Colleuil, B., Profizi, J.P., Dossou, C., 1980. Le lac Nokoué, environnement du
950 domaine margino-littoral sud-béninois : bathymétrie, lithofaciès, salinité, mollusque
951 et peuplements végétaux. Bull. Inst. Géol. Bass. Aguit.. Bordeaux 28, 115-142.
952 Torrence, C., Compo, G.P., 1998. A Practical Guide to Wavelet Analysis. Bull. Am. Met. Soc.
953 79, 61-78.
954 Valiela, I., 1995. Marine Ecological Processes, second ed. Springer-Verlag, New York.
955 Varlet, F., 1978. Le régime de la lagune Ébrié, Côte-d'Ivoire. Traits physiques essentiels.
956 Paris, Travaux et Documents essentiels de l'Orstom, 83, 162 pp.
957 Veleda, D., Montagne, R., Araujo, M., 2012. Cross-Wavelet Bias Corrected by Normalizing
958 Scales, Journal of Atmospheric and Oceanic Technology 29 (9), 1401-1408.
959 Ward, P.R.B., 1979. Seiches, tides and wind set-up on Lake Kariba. Limnol. Oceanogr. 24,
960 151-157. 261.
961 Wilson, G.V., Rigby, J.R., Ursic, M., Dabney, S.M., 2016. Soil pipe flow tracer experiments:
962 1. Connectivity and transport characteristics. Hydrology processes 30, 1265-1279.
963 World Bank, 2011. Inondations au Benin: Rapport d'Evaluation des Besoins Post
964 Catastrophe. World Bank: Washington, DC, USA. available at :
965 http://documents1.worldbank.org/curated/en/750141468208769683/pdf/694130
966 ESW0P1240lood0Recovery0Report.pdf (last access: December 24, 2020).
967 Zandagba, J., Moussa, M., Obada, E., Afouda, A., 2016. Hydrodynamic Modeling of Nokoué
968 Lake in Benin. Hydrology 2016, 3, 44.
969